

Magnetic “Molecular Oligomers” Based on Decametallic Supertetrahedra: A Giant Mn_{49} Cuboctahedron and its $\text{Mn}_{25}\text{Na}_4$ Fragment

Maria Manoli, Sofia Alexandrou, Linh Pham, Giulia Lorusso, Wolfgang Wernsdorfer, Marco Evangelisti, George Christou, and Anastasios J. Tasiopoulos*

Abstract: Two nanosized Mn_{49} and $\text{Mn}_{25}\text{Na}_4$ clusters based on analogues of the high-spin ($S=22$) $[\text{Mn}^{\text{III}}_6\text{Mn}^{\text{II}}_4(\mu_4\text{-O})_4]^{18+}$ supertetrahedral core are reported. Mn_{49} and $\text{Mn}_{25}\text{Na}_4$ complexes consist of eight and four decametallic supertetrahedral subunits, respectively, display high virtual symmetry (O_h), and are unique examples of clusters based on a large number of tightly linked high nuclearity magnetic units. The complexes also have large spin ground-state values (Mn_{49} : $S=61/2$; $\text{Mn}_{25}\text{Na}_4$: $S=51/2$) with the Mn_{49} cluster displaying single-molecule magnet (SMM) behavior and being the second largest reported homometallic SMM.

The construction of giant metal clusters based on tightly connected, magnetically interesting, polynuclear complexes is one of the most important challenges for coordination chemists. Interest in such compounds stems not only from their impressive structural features, such as large size, high symmetry, beautiful shapes, and architectures, but also from the possibility that the magnetic properties of their structural subunits can be retained or even enhanced in the large polynuclear assembly. Although several giant metal–organic compounds have been reported, the structures of both the homometallic (for example, Mn_{84} ,^[1] Mn_{44} ,^[2] Mn_{32} ,^[3–5] Fe_{64} ,^[6] Fe_{42} ,^[7] Co_{36} ,^[8] Cu_{44} ,^[9] Pd_{84} ,^[10] and Ln_{104} ($\text{Ln} = \text{Nd}, \text{Gd}$)^[11]) and heterometallic (for example, $\text{Mn}_{36}\text{Ni}_{14}$,^[12] $\text{Cu}_{17}\text{Mn}_{28}$,^[13] $[\text{Ni}_{12}(\text{Cr}_7\text{Ni})_6]$,^[14] $\text{Ni}_{60}\text{La}_{76}$,^[15] $\text{Ni}_{54}\text{Gd}_{54}$,^[16] $\text{Cu}_{36}\text{Ln}_{24}$ ($\text{Ln} = \text{Gd}, \text{Dy}$)^[17]) complexes contain mainly oligonuclear, usually

trinuclear (such as oxo or hydroxo-centered triangles) and tetranuclear (such as cubanes) subunits. There are also a few examples of nanosized clusters based on subunits that have not been isolated in a discrete form and only a couple of complexes displaying building units or fragments that have been reported in the literature. Such examples are the Fe_{64} cluster based on an Fe_8 subunit^[6] and the Mn_{84} wheel which contains a Mn_{11} fragment reported in the past, although its true repeating unit is a Mn_{14} cluster never seen in discrete form.^[11] Although the synthesis of most giant metal–organic clusters is a very complicated process based to some extent on serendipity, a discussion has been initiated in the literature concerning the possibility to predict the structure and nuclearity of metal–organic clusters that could be targeted and prepared by future generations of chemists.^[10,18] It would be tempting to assume, for example, that stable structural units easily assembled in the reaction solution under various conditions could be linked in the presence of the proper bridging ligands giving rise to a library of theoretically predicted high nuclearity clusters. However, so far there is no experimental proof to support this expectation.

One ideal structural type to act as a building block in high nuclearity clusters is the $[\text{Mn}^{\text{III}}_6\text{Mn}^{\text{II}}_4(\mu_4\text{-O})_4]^{18+}$ supertetrahedral core which combines a beautiful, high symmetry (T_d) metal topology and interesting magnetic properties.^[19] In addition, it has been stabilized in discrete form with several ligands^[19–21] and under various reaction conditions, and has appeared as the repeating unit in zero-dimensional Mn_{17} ,^[22,23] and Mn_{19} ,^[24] clusters and in the giant $\text{Mn}_{36}\text{Ni}_{14}$ “loop-of-loops and supertetrahedra” aggregate,^[12] all containing two $\text{Mn}^{\text{III}}_6\text{Mn}^{\text{II}}_4$ supertetrahedral units. Most of the compounds possessing this core display ferromagnetic exchange interactions and large or even giant ground-state spin values, which for the Mn_{10} , Mn_{17} , Mn_{19} , and $\text{Mn}_{36}\text{Ni}_{14}$ clusters mentioned above are $S=22$, 37, 83/2, and 26, respectively. However, there is no cluster containing more than two $\text{Mn}^{\text{III}}_6\text{Mn}^{\text{II}}_4$ supertetrahedral subunits.

Herein we report the compounds $[\text{Mn}^{\text{III}}_{36}\text{Mn}^{\text{II}}_{13}(\mu_4\text{-O})_{32}(\mu_3\text{-OCH}_3)_8(\mu_3\text{-hp})_{24}(\text{O}_2\text{CH})_6(\text{DMF})_{12}(\text{OH})_8$ (**1**) and $[\text{Mn}^{\text{III}}_{20}\text{Mn}^{\text{II}}_{15}\text{Na}_4(\mu_4\text{-O})_{16}(\mu_3\text{-OCH}_3)_4(\mu_3\text{-hp})_{16}(\text{O}_2\text{CCH}_3)_4(\text{O}_2\text{CH})(\text{DMF})_8(\text{O}_2\text{CH})$ (**2**; $\text{H}_2\text{hp} = 2\text{-(hydroxymethyl)phenol}$, $\text{DMF} = \text{dimethylformamide}$) consisting of eight and four fused M_{10} supertetrahedral units, respectively. Both compounds display highly symmetric, nanosized structural cores (O_h virtual symmetry), with that of **1** describing an “Archimedean solid” called a cuboctahedron. Additionally, the compounds are structurally related, with the core of **2** being

[*] Dr. M. Manoli, S. Alexandrou, Dr. A. J. Tasiopoulos
Department of Chemistry, University of Cyprus
1678 Nicosia (Cyprus)
E-mail: atasio@ucy.ac.cy

Dr. L. Pham,^[†] Prof. G. Christou
Department of Chemistry, University of Florida
Gainesville, FL 32611-7200 (USA)

Dr. G. Lorusso, Dr. M. Evangelisti
Instituto de Ciencia de Materiales de Aragón and Departamento de Física de la Materia Condensada, CSIC-Universidad de Zaragoza
50009 Zaragoza (Spain)

Dr. W. Wernsdorfer
Institut Neel, CNRS, BP 166
25 Avenue des Martyrs, 38042 Grenoble Cedex 9 (France)

[†] Current address: Texas A&M University-Central Texas
Department of Science and Mathematics, Killeen, TX 76549 (USA)

Supporting information for this article (including full experimental details for the synthesis and characterization of the reported complexes) is available on the WWW under <http://dx.doi.org/10.1002/anie.201509461>.

almost identical to a fragment of that of **1**. Magnetism studies revealed the existence of dominant ferromagnetic exchange interactions in both **1** and **2** leading to ground-state spin values of 61/2 and 51/2, respectively. In addition, the magnetocaloric effect for both complexes is seen to develop over a significantly wide temperature range. Finally, compound **1** displays single-molecule magnet (SMM) behavior and is the second largest homometallic 3d SMM reported to date.

Both compounds discussed herein were prepared from the investigation of reactions of Mn salts with H₂hp under various conditions. Thus, the reaction of [Mn(ClO₄)₂] \cdot xH₂O, H₂hp, NaOCN, and Bu₄N(ClO₄) in a 1:1:1:1 molar ratio in a DMF/MeOH solvent mixture led to the isolation of **1** \cdot 10DMF in 20% yield after approximately 2 months. Compound **2**-DMF was isolated in 25% yield from the reaction of Mn(acac)₂ with H₂hp in the presence of NaOMe in a 1:1:2 molar ratio in a DMF/MeOH solvent mixture.

The asymmetric unit of **1**^[25] consists of two independent quarters of the Mn₄₉ cation (Figure 1a), as well as OH[−] counterions and solvent molecules of crystallization. The two Mn₄₉ units are nearly identical, and display a centrosymmetric, mixed-valent [Mn^{III}₃₆Mn^{II}₁₃(μ₄-O)₃₂]⁷⁰⁺ structural core (Figure 1b). The latter consists of eight [Mn^{III}₆Mn^{II}₄(μ₄-O)₄]¹⁸⁺ supertetrahedral subunits (Figure 1b, right) all having a common apical Mn²⁺ ion and each of them sharing three edges with three other neighboring supertetrahedra. The assembly of the eight Mn₁₀ supertetrahedra results in a geometrical 3D shape consisting of six square pyramids sharing their triangular faces with eight tetrahedra. The Mn₄₉ polyhedron thus has eight triangular and six square faces and describes an “Archimedean solid” called a cuboctahedron (Figure 1c). The 12 Mn²⁺ ions define the vertices of the cuboctahedron and 24 Mn³⁺ ions are located on its edges. The rest of the Mn³⁺ (twelve) and Mn²⁺ (one) ions of **1** are found on the inner edges of the supertetrahedra and at the center of the cuboctahedron, respectively. The μ₄-O^{2−} ions of the Mn₄₉ cluster bridge one Mn²⁺ and three Mn³⁺ ions as has been seen in other structures containing the [Mn^{III}₆Mn^{II}₄(μ₄-O)₄]¹⁸⁺ supertetrahedral core,^[19–24] whereas the μ₃-MeO[−] ligands bridge three Mn³⁺ ions. The peripheral ligation is completed by 24 fully deprotonated hp^{2−} ligands connecting two Mn²⁺ and one Mn³⁺ ions in a η²:η²-μ₃ mode, six severely disordered HCO₂[−] ligands bridging exclusively Mn³⁺ ions, and 12 terminal DMF molecules bound to the 12 outer Mn²⁺ ions.

The asymmetric unit of **2**-DMF^[25] consists of one quarter of the cation of **2** (Figure 2a) and lattice counterions and solvent molecules. Its [Mn^{III}₂₀Mn^{II}₅Na₄(μ₄-O)₁₆]⁴²⁺ core (Figure 2b) consists of four [Mn^{III}₆Mn^{II}₃Na(μ₄-O)₄]¹⁷⁺ supertetrahedral units having a common Mn²⁺ ion occupying their apical position and each of them sharing two edges with two other neighboring supertetrahedra. The overall shape of the core can be described as a square pyramid sharing each of its triangular faces with a supertetrahedron. The Mn²⁺ ions occupy the common vertices of the square pyramid and the supertetrahedra and the Na⁺ ions the remaining vertices of the four supertetrahedra. Sixteen Mn³⁺ ions are located on the outer edges of the four supertetrahedra and four on their

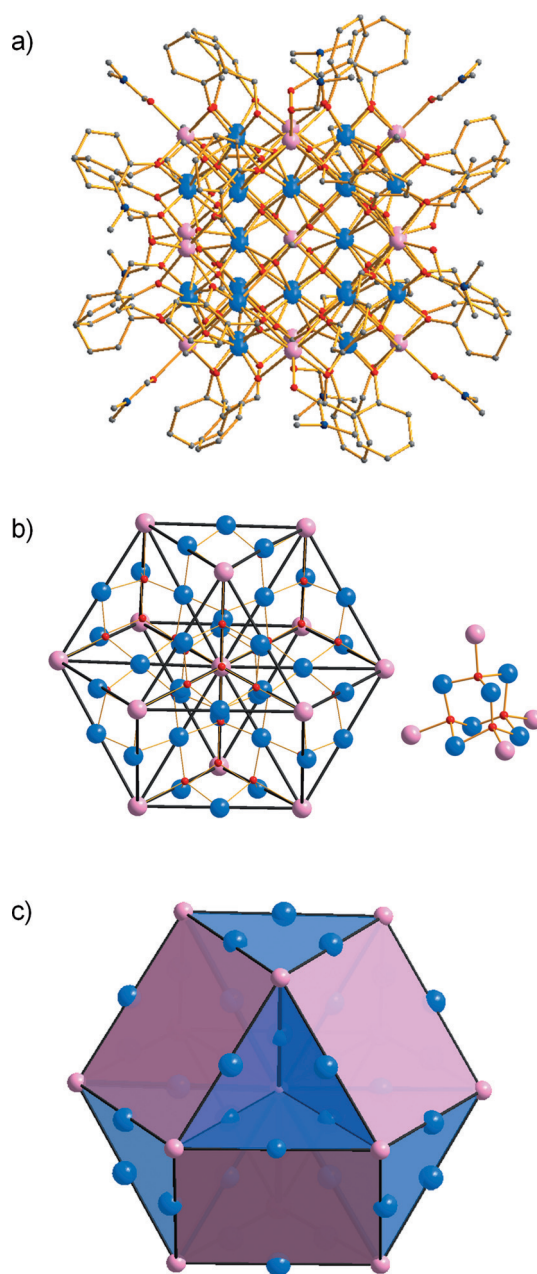


Figure 1. a) The molecular structure of the cation of **1**, b) the [Mn^{III}₃₆Mn^{II}₁₃(μ₄-O)₃₂]⁷⁰⁺ structural core (left) and the [Mn^{III}₆Mn^{II}₄(μ₄-O)₄]¹⁸⁺ supertetrahedral subunit (right), and c) the Mn₄₉ metallic skeleton. The solid black lines connecting the Mn ions in (b; left) and (c) and the colored planes in (c) are used to emphasize the existence of eight Mn^{III}₆Mn^{II}₄ supertetrahedral subunits and the cuboctahedral shape of complex **1**. Color code: Mn³⁺ = blue, Mn²⁺ = pink, O = red, N = dark blue, C = gray.

inner edges (in the common faces of the square pyramid and the four supertetrahedra). The core of **2** is related to that of **1** and in particular it is almost equal to a fragment of the core of **1**. In fact, the core of **1** can be described as consisting of two M₂₉ units of **2** sharing a central M₉ plane (Figure 3). As a result, structural features, such as the bridging modes of the ligands, the coordination environment, and number of metal ions, in **2** are similar to those described for **1**. Thus, each

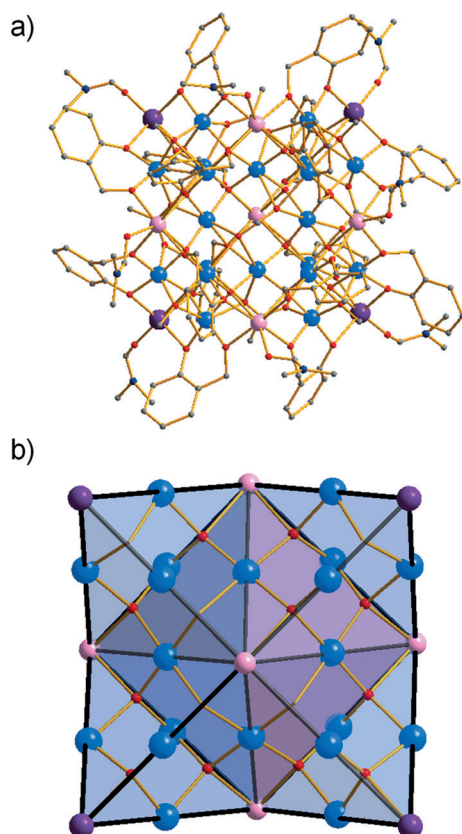


Figure 2. a) The molecular structure and b) the $[\text{Mn}^{\text{III}}_{20}\text{Mn}^{\text{II}}_5\text{Na}_4(\mu_4\text{-O})_{16}]^{42+}$ structural core of the cation of **2**. The colored planes in (b) and the solid black lines connecting the Mn ions are used to emphasize the shape of the core of **2** (see the text for details). Color code: Mn^{3+} = blue, Mn^{2+} = pink, Na^+ = purple, O = red, N = dark blue, C = gray.

of the sixteen O^{2-} ions of the core is linked to three Mn^{3+} and one Mn^{2+} or Na^+ ions, the four MeO^- groups to three Mn^{3+} ions, and the sixteen hp^{2-} ligands bridge in a $\eta^1:\eta^2-\mu_3$ mode either $\text{Mn}^{2+}/\text{Na}^+/\text{Mn}^{3+}$ or 2 $\text{Mn}^{2+}/\text{Mn}^{3+}$ ions. The peripheral ligation is completed by four acetate ligands bridging in a $\eta^1:\eta^3-\mu_4$ mode, a severely disordered formate ion, and eight terminal DMF molecules connected to the Mn^{2+} and Na^+ ions.

The oxidation states of the Mn ions and the protonation level of $\text{O}^{2-}/\text{RO}^-$ ligands in **1** and **2** were determined by bond valence sum (BVS) calculations, charge considerations, and inspection of metric parameters.^[26,27] All octahedral Mn^{3+} ions display a Jahn–Teller (JT) elongation with the carboxylate O and $\mu_3\text{-MeO}^-$ located on the JT axes, which however are not coparallel.

Interestingly, the cores of **1** and **2** are also related to the $[\text{Mn}^{\text{III}}_{11}\text{Mn}^{\text{II}}_6(\mu_4\text{-O})_8]^{29+}$ core of a family of Mn_{17} clusters reported in 2009 (see Figure 3 and Figure S4 in the Supporting Information).^[22,23] These Mn_{17} clusters consist of two edge-sharing $[\text{Mn}^{\text{III}}_6\text{Mn}^{\text{II}}_4(\mu_4\text{-O})_4]^{18+}$ supertetrahedral units and display ferromagnetic exchange interactions. In fact, one of these Mn_{17} analogues combines an $S=37$ spin ground state and SMM behavior and is the largest-spin SMM reported.^[22] Complex **2** contains two $[\text{Mn}^{\text{III}}_{11}\text{Mn}^{\text{II}}_6(\mu_4\text{-O})_8]^{29+}$ fragments,

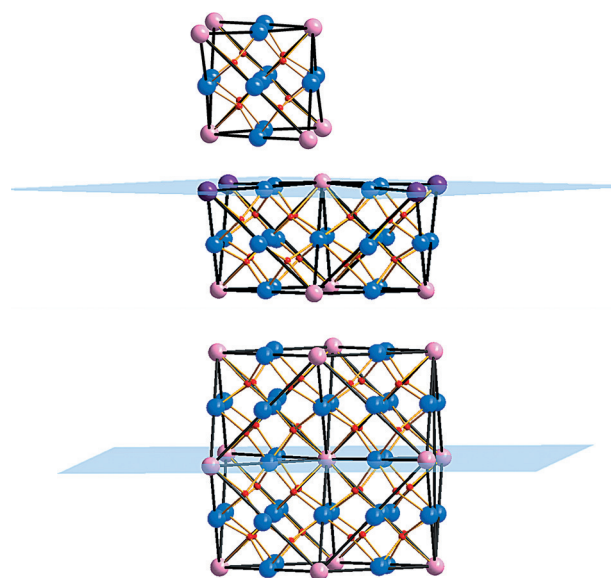


Figure 3. Representations of the structural cores of **1** (bottom), **2** (middle), and a reported Mn_{17} cluster^[22,23] (top; see text for details), respectively, highlighting their structural relationship. The light blue planes through the cores of **1** and **2** are used to emphasize the common M_5 plane of the two M_{29} subunits, related to the structure of **2**, within the M_{49} cuboctahedral core of **1** (see the text for details). Color code: Mn^{3+} = blue, Mn^{2+} = pink, Na^+ = purple, O = red.

nearly identical to the core of the above discussed Mn_{17} cluster, sharing a M_5 plane, whereas complex **1** consists of four such units sharing two M_5 planes with their neighboring units. Both **1** and **2** are nanosized clusters and among the largest discrete (0D) 3d metal clusters with maximum dimensions of about 2.5 and 2.2 nm and molecular weights of approximately 8400 and 4800 g mol^{-1} , respectively, with compound **1** being smaller only than Mn_{84} and Fe_{64} clusters.^[1,6]

Direct-current (dc) magnetic susceptibility (χ_M) measurements were performed on powdered crystalline samples of **1**·10DMF and **2**·DMF in the 5–300 K temperature range in a 0.1 T magnetic field. The data are plotted as $\chi_M T$ versus T in Figure 4a. $\chi_M T$ values for **1**·10DMF and **2**·DMF increase steadily from 189.6 and 101.4 $\text{cm}^3 \text{mol}^{-1} \text{K}$, respectively, at 300 K, to maxima of 536.8 (at 20 K; for **1**) and 367.2 $\text{cm}^3 \text{mol}^{-1} \text{K}$ (at 10 K; for **2**) before decreasing to 431.5 and 337.9 $\text{cm}^3 \text{mol}^{-1} \text{K}$ at 5.0 K. The $\chi_M T$ maxima suggest ground-state spin values $S=63/2 \pm 1$ and $53/2 \pm 1$ for **1**·10DMF and **2**·DMF, respectively, and the overall data indicate the existence of dominant ferromagnetic exchange interactions in both complexes (see the Supporting Information for a more detailed discussion). The abrupt decrease of $\chi_M T$ values at very low temperatures for both complexes is assigned to zero-field splitting (ZFS), Zeeman effects from the applied field, and/or weak intermolecular interactions.

To further probe the ground-state spin of the two complexes, magnetization (M) versus dc field measurements at applied magnetic fields (H) and temperatures in the 1–70.0 kG and 1.8–10.0 K ranges, respectively, were performed (see the Supporting Information for a more detailed discussion). The data are shown in Figures S9 and S10 for **1**·10DMF and **2**·DMF, respectively, as reduced magnetization

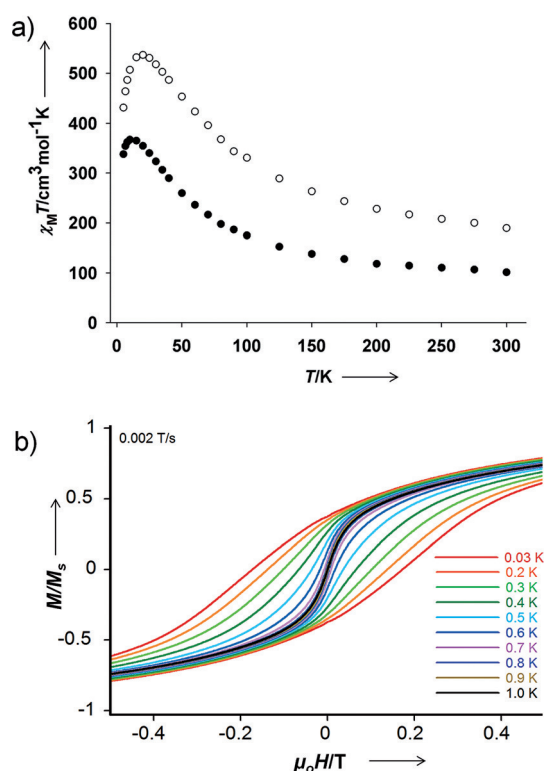


Figure 4. a) $\chi_{\text{M}}T$ versus T plot for complex **1·10DMF** (open circles) and **2·DMF** (solid circles) at 0.1 T and b) magnetization (M) versus applied magnetic field ($\mu_0 H$) hysteresis loops for a single crystal of **1·10DMF** at the indicated temperatures and a fixed field sweep rate of 0.002 T s^{-1} . The magnetization is normalized to its saturation value (M_{S}).

($M/N\mu_{\text{B}}$) versus H/T plots, where N is Avogadro's number and μ_{B} is the Bohr magneton. The data were fit by assuming that only the ground state is populated at these temperatures and magnetic fields, and by including isotropic Zeeman interactions and axial zero-field splitting ($D\hat{S}_z^2$). Using only data collected at low fields to minimize problems from low-lying excited states, satisfactory fits were obtained (solid lines in Figures S9 and S10) with $S = 61/2$, $g = 1.99(1)$, and $D = -0.01 \text{ cm}^{-1}$ for **1·10DMF**, and $S = 51/2$, $g = 1.99(1)$, and $D = -0.01 \text{ cm}^{-1}$ for **2·DMF**. Alternative fits with slightly higher or lower S values gave for both compounds unreasonable g and D values.

Prompted by the large magnetization values detected in both complexes, we performed magnetocaloric studies to investigate their cooling capability. A complete discussion about these investigations is provided in the Supporting Information. In comparison to the magnetocaloric effect (MCE) reported for other molecular compounds,^[28] the data revealed moderate entropy changes for both complexes, that is, $-\Delta S_{\text{m}} = 6.4 \text{ J kg}^{-1} \text{ K}^{-1}$ at $T = 10 \text{ K}$ and $\mu_0 \Delta H = 7 \text{ T}$ (where μ_0 is the vacuum permeability) for **1·10DMF** and $-\Delta S_{\text{m}} = 7.7 \text{ J kg}^{-1} \text{ K}^{-1}$ at $T = 8 \text{ K}$ and $\mu_0 \Delta H = 7 \text{ T}$ for **2·DMF** (Figure S8). Interestingly, the entropy changes remain almost constant from 30 K to 5 K ($\mu_0 \Delta H = 7 \text{ T}$), indicating that both compounds display cooling capability for a significantly wide range of temperatures. It is also notable that the zero-field

entropies for both complexes (Figure S6) are consistent with the afore-discussed ground-state spin values. On the basis of the magnetization data, assuming that only $S = 61/2$ is populated below 2 K for **1·10DMF** ($S = 51/2$ for **2·DMF**) would imply a value for the zero-field magnetic entropy at 2 K close to $R \ln(2S + 1) = 4.1R$ ($4.0R$ for **2·DMF**), where R is the gas constant, as indeed measured (Figure S6).

Alternating-current (ac) magnetic susceptibility measurements were performed in the 1.8–10 K temperature range in zero applied dc field and a 3.5 G ac field oscillating at 50–1000 Hz. The plots of the in-phase component of the ac susceptibility $\chi'_{\text{M}}T$ versus T and the out-of-phase susceptibility χ''_{M} versus T for **1·10DMF** and **2·DMF** are shown in Figures S11 and S12. Extrapolation of the $\chi'_{\text{M}}T$ data from above 6.0 K to 0 K, at which point only the ground state will be populated (avoiding the lower temperature data that will be affected by intermolecular dipolar interactions), gives values of approximately 460 and $360 \text{ cm}^3 \text{ mol}^{-1} \text{ K}$. These values are consistent with $S = 61/2 \pm 1$ and $51/2 \pm 1$ ground states for **1·10DMF** and **2·DMF**, respectively, with $g \approx 2.00$, confirming the conclusions from the dc studies. The out-of-phase plot of **1·10DMF** displays weak χ''_{M} signals below 2.6 K, suggestive of the presence of slow relaxation of the magnetization. No out-of-phase signals were observed for **2·DMF**.

Encouraged by the observation of out-of-phase signals in **1·10DMF**, we carried out, using a micro-SQUID apparatus, single-crystal hysteresis studies to confirm that it indeed displays SMM behavior. The obtained magnetization versus dc field data at different temperatures and a fixed field sweep rate of 0.002 T s^{-1} are shown in Figure 4b, and at different scan rates and a constant $T = 0.5 \text{ K}$ in Figure S13. Hysteresis loops appeared below 1 K whose coercivities increase with decreasing temperature and increasing field scan rates, as expected for SMMs. Thus, **1·10DMF** is a new SMM, with a blocking temperature of 1 K, above which no hysteresis is observed. The hysteresis loops do not contain any steps characteristic of quantum tunneling of the magnetization (QTM); however this is typical for higher nuclearity SMMs where the steps are smeared out due to various effects, such as the existence of low-lying excited states and intermolecular interactions.^[1,2] Magnetization versus time decay data were collected on a single crystal of **1·10DMF** to assess the magnetization relaxation dynamics, and the results are shown in Figure S14. These data were used to calculate the relaxation rates ($1/\tau$, where τ is the lifetime) at different temperatures and to construct the Arrhenius plot (shown as τ versus $1/T$ in Figure S15) based on the Arrhenius equation:

$$\tau = \tau_0 \exp(U_{\text{eff}}/kT) \quad (1)$$

where τ_0 is the pre-exponential factor, U_{eff} is the effective relaxation barrier, and k is the Boltzmann constant. The fit to the thermally activated region above about 0.1 K gave $\tau_0 = 7 \times 10^{-14} \text{ s}$ and $U_{\text{eff}} = 19 \text{ K}$. The small value of τ_0 , smaller than is typical for purely SMM behavior, is attributed to the low-lying excited states and the weak intermolecular interactions and is a common situation for large clusters.^[2,22,23,29] At about 0.1 K and below, the relaxation becomes temperature-independent as expected for relaxation by ground-state QTM,

that is, via the $M_S = \pm 61/2$ levels of the $S = 61/2$ spin manifold.

In summary, two nanosized $Mn_{25}Na_4$ and Mn_{49} molecular aggregates based on four and eight $[Mn^{III}_6Mn^{II}_3M(\mu_4-O)_4]^{n+}$ ($M = Mn^{II}$, $n = 18$, **1**-10DMF; $M = Na^+$, $n = 17$, **2**-DMF) supertetrahedral repeating units are reported. This extended conjunction of decametallic supertetrahedra afforded structural cores displaying high symmetry (O_h) and aesthetically pleasing 3D solid shapes including an Archimedean shape, called a cuboctahedron. Compounds **1** and **2** also display dominant ferromagnetic exchange interactions and spin ground-state values $S = 61/2$ and $51/2$, respectively, that are among the largest reported for high nuclearity metal clusters.^[7,22–24,29] Complex **1** was also found to behave as a SMM and thus it is the second largest Mn cluster and homometallic SMM reported.^[1]

It should be pointed out that although compounds containing the $[Mn^{III}_6Mn^{II}_4(\mu_4-O)_4]^{18+}$ supertetrahedral core are often found to display entirely ferromagnetic exchange interactions and the maximum possible spin ground states,^[19–22,24] this is not the case for **1** and **2**, in which the corresponding maximum values would be, by far, record values of $S = 209/2$ and $105/2$, respectively. Obviously in the case of these two compounds, apart from the exchange interactions within the decametallic supertetrahedral core which are expected to be ferromagnetic, there are also additional couplings between the neighboring M_{10} repeating units, some of which are antiferromagnetic. For this reason, although predominant ferromagnetic behavior was realized for both complexes, the spin ground states observed are significantly lower than the maximum possible values. However, these magnetic systems have the potential to display larger S values if some of the antiferromagnetic interactions are switched to ferromagnetic ones by synthesizing analogues of **1** and **2** with slightly different structural parameters, such as bond lengths and angles and peripheral ligation, as was accomplished in the past for other magnetic systems.^[29] These compounds are also the first molecular species containing more than two repeating decametallic supertetrahedra and their cores are related to each other and also to that of the Mn_{17} “dimeric” analogues consisting of two edge-sharing decametallic supertetrahedra. Thus, **1** and **2** can be considered as the “octamer” and “tetramer”, respectively, of the well-known decametallic supertetrahedra, and their isolation reveals that other molecular oligomers based on a large number of repeating high nuclearity clusters are possible. Synthetic investigations targeting larger analogues of this series of molecular oligomers, such as the dodecamer and the hexadecamer, are in progress. Indisputably, this study opens up new directions in metal cluster chemistry towards the construction of giant metal clusters with fascinating crystal structures and magnetic properties.

Acknowledgements

This work was supported by the Cyprus Research Promotion Foundation grant ANABAΘMIS/IIAΓIO/0308/12 which is co-funded by the Republic of Cyprus and the European Regional Development Fund, the US National Science

Foundation (Grant DMR-1213030 to G.C.), and the Spanish MINECO (Project FEDER-MAT2012-38318-C03-01).

Keywords: cluster compounds · magnetic properties · manganese · O ligands · single-molecule magnets

How to cite: *Angew. Chem. Int. Ed.* **2016**, *55*, 679–684
Angew. Chem. **2016**, *128*, 689–694

- [1] A. J. Tasiopoulos, A. Vinslava, W. Wernsdorfer, K. A. Abboud, G. Christou, *Angew. Chem. Int. Ed.* **2004**, *43*, 2117–2121; *Angew. Chem.* **2004**, *116*, 2169–2173.
- [2] E. E. Moushi, C. Lampropoulos, W. Wernsdorfer, V. Nastopoulos, G. Christou, A. J. Tasiopoulos, *J. Am. Chem. Soc.* **2010**, *132*, 16146–16155.
- [3] R. T. W. Scott, S. Parsons, M. Murugesu, W. Wernsdorfer, G. Christou, E. K. Brechin, *Angew. Chem. Int. Ed.* **2005**, *44*, 6540–6543; *Angew. Chem.* **2005**, *117*, 6698–6701.
- [4] S. K. Langley, R. A. Stott, N. F. Chilton, B. Moubaraki, K. S. Murray, *Chem. Commun.* **2011**, *47*, 6281–6283.
- [5] M. Manoli, R. Inglis, M. J. Manos, V. Nastopoulos, W. Wernsdorfer, E. K. Brechin, A. J. Tasiopoulos, *Angew. Chem. Int. Ed.* **2011**, *50*, 4441–4444; *Angew. Chem.* **2011**, *123*, 4533–4536.
- [6] T. Liu, Y.-J. Zhang, Z.-M. Wang, S. Gao, *J. Am. Chem. Soc.* **2008**, *130*, 10500–10501.
- [7] S. Kang, H. Zheng, T. Liu, K. Hamachi, S. Kanegawa, K. Sugimoto, Y. Shiota, S. Hayami, M. Mito, T. Nakamura, M. Nakano, M. L. Baker, H. Nojiri, K. Yoshizawa, C. Duan, O. Sato, *Nat. Commun.* **2015**, *6*, 5955–5960.
- [8] P. Alborés, E. Rentschler, *Angew. Chem. Int. Ed.* **2009**, *48*, 9366–9370; *Angew. Chem.* **2009**, *121*, 9530–9534.
- [9] M. Murugesu, R. Clérac, C. E. Anson, A. K. Powell, *Inorg. Chem.* **2004**, *43*, 7269–7271.
- [10] F. Xu, H. N. Miras, R. A. Scullion, D.-L. Long, J. Thiel, L. Cronin, *Proc. Natl. Acad. Sci. USA* **2012**, *109*, 11609–11612.
- [11] J.-B. Peng, X.-J. Kong, Q.-C. Zhang, M. Orendáč, J. Prokleška, Y.-P. Ren, L.-S. Long, Z. Zheng, L.-S. Zheng, *J. Am. Chem. Soc.* **2014**, *136*, 17938–17941.
- [12] M. Charalambous, E. E. Moushi, C. Papatriantafyllopoulou, W. Wernsdorfer, V. Nastopoulos, G. Christou, A. J. Tasiopoulos, *Chem. Commun.* **2012**, *48*, 5410–5412.
- [13] W.-G. Wang, A.-J. Zhou, W.-X. Zhang, M.-L. Tong, X.-M. Chen, M. Nakano, C. C. Beedle, D. N. Hendrickson, *J. Am. Chem. Soc.* **2007**, *129*, 1014–1015.
- [14] G. F. S. Whitehead, F. Moro, G. A. Timco, W. Wernsdorfer, S. J. Teat, R. E. P. Winpenny, *Angew. Chem. Int. Ed.* **2013**, *52*, 9932–9935; *Angew. Chem.* **2013**, *125*, 10116–10119.
- [15] X.-J. Kong, L.-S. Long, R.-B. Huang, L.-S. Zheng, T. D. Harris, Z. Zheng, *Chem. Commun.* **2009**, 4354–4356.
- [16] X.-J. Kong, Y.-P. Ren, W.-X. Chen, L.-S. Long, Z. Zheng, R.-B. Huang, L.-S. Zheng, *Angew. Chem. Int. Ed.* **2008**, *47*, 2398–2401; *Angew. Chem.* **2008**, *120*, 2432–2435.
- [17] J.-D. Leng, J.-L. Liu, M.-L. Tong, *Chem. Commun.* **2012**, *48*, 5286–5288.
- [18] G. F. S. Whitehead, J. Ferrando-Soria, L. G. Christie, N. F. Chilton, G. A. Timco, F. Moro, R. E. P. Winpenny, *Chem. Sci.* **2014**, *5*, 235–239.
- [19] T. C. Stamatatos, K. A. Abboud, W. Wernsdorfer, G. Christou, *Angew. Chem. Int. Ed.* **2006**, *45*, 4134–4137; *Angew. Chem.* **2006**, *118*, 4240–4243.
- [20] M. Manoli, R. D. L. Johnstone, S. Parsons, M. Murrie, M. Affronte, M. Evangelisti, E. K. Brechin, *Angew. Chem. Int. Ed.* **2007**, *46*, 4456–4460; *Angew. Chem.* **2007**, *119*, 4540–4544.
- [21] S. Nayak, M. Evangelisti, A. K. Powell, J. Reedijk, *Chem. Eur. J.* **2010**, *16*, 12865–12872.

- [22] E. E. Moushi, T. C. Stamatatos, W. Wernsdorfer, V. Nastopoulos, G. Christou, A. J. Tasiopoulos, *Inorg. Chem.* **2009**, *48*, 5049–5051.
- [23] S. Nayak, L. M. C. Beltran, Y. Lan, R. Clérac, N. G. R. Hearn, W. Wernsdorfer, C. E. Anson, A. K. Powell, *Dalton Trans.* **2009**, 1901–1903.
- [24] A. M. Ako, I. J. Hewitt, V. Mereacre, R. Clérac, W. Wernsdorfer, C. E. Anson, A. K. Powell, *Angew. Chem. Int. Ed.* **2006**, *45*, 4926–4929; *Angew. Chem.* **2006**, *118*, 5048–5051.
- [25] Crystallographic data for **1**·10DMF and **2**·DMF are provided in the Supporting Information. CCDC 1422256 (**1**·10DMF) and 1422257 (**2**·DMF) contain the supplementary crystallographic data for this paper. These data are provided free of charge by The Cambridge Crystallographic Data Centre.
- [26] W. Liu, H. H. Thorp, *Inorg. Chem.* **1993**, *32*, 4102–4105.
- [27] I. D. Brown, D. Altermatt, *Acta Crystallogr. Sect. B* **1985**, *41*, 244–247.
- [28] “Molecule-based magnetic coolers: Measurement, design and application”: M. Evangelisti in *Molecular Magnets, NanoScience and Technology* (Eds.: J. Bartolomé, F. Luis, J. F. Fernández), Springer, Berlin, Heidelberg, **2014**, pp. 365–387.
- [29] T. C. Stamatatos, K. A. Abboud, W. Wernsdorfer, G. Christou, *Angew. Chem. Int. Ed.* **2007**, *46*, 884–888; *Angew. Chem.* **2007**, *119*, 902–906.

Received: October 9, 2015

Published online: November 27, 2015